Microstrip Antenna Array Design for Unmanned Aerial Vehicles Detection Radar

Pedro Mendes Ruiz[1*], Xavier Begaud[2], François Magne[3], Etienne Leder[1], Antoine Khy[2]

[1] Bowen ERTE-ETSA, Les Ulis, France
[2] LTCI, Télécom Paris, Institut Polytechnique de Paris, Palaiseau, France
[3] When-AB, Paris, France

Corresponding author: Pedro Mendes Ruiz (e-mail: pmruiz4@gmail.com).

ABSTRACT This work presents the design and realization of four linear arrays of microstrip rectangular patch antennas. This linear array is one of the elements of a passive radar using signals from 4G base stations for UAV detection. The arrays have been validated and operate from 2.62 GHz to 2.69 GHz, with a HPBW of 82° in H-plane and a maximal gain going from 11.1 dB to 12.2 dB in the required bandwidth, with a cosecant squared pattern in the E-plane.

INDEX TERMS Microstrip antenna, Antenna array, Genetic algorithm, Beamforming, UAV Detection.

I. INTRODUCTION

THE threat of easy-to-deploy low-cost drones requires an advanced detection for the protection of sensible sites (e.g. airport runways, stadiums, industrial sites). The goal of the DIOD™ project (Detection & Identification Of Drones) is to develop a passive radar that uses 4G base stations as remote continuous transmitters. This work presents the design of the receiving antenna developed in the framework of the FUI (Fond Unique Interministériel) DIOD project.

Many solutions exist to detect the presence of drones with mechanical, optical, or antenna array based solutions [1].

Directive antennas are used by radar systems for the detection of drones. The high gain from a directional antenna helps to achieve long-range and the narrow beam may be used to estimate the position of the aerial vehicle. Traditional radar antennas were simple parabolic reflectors and Cassegrain feed parabolic reflectors that were mechanically rotated. Today, phased arrays are used to suppress mechanical rotation. The phased arrays are further divided into active and passive types [2]. The size and shape of the active electronically scanned array and passive electronically scanned array are similar. To obtain a very directional beam, you need a large number of elements and when the choice of frequency is free, the use of the millimeter band is interesting, for instance, due to the reduced dimensions of the radiating elements [3].

In passive radars, different antennas can be used. It is possible to use an antenna with a low directivity like the quasi-yagi antenna [4] but the range will be reduced. Other solutions using horns make it possible to cover a large area but the antenna is complex to achieve [5].

Passive detection of UAV can be obtained by using multiple antennas and DOA estimation [6], [7]. The goal of the DIOD project is to use an array of a dozen linear columns to ensure permanent detection in 24 directions by beamforming. In this article, the design and validation of a third of the global array is presented. Each linear array is designed to produce a cosecant squared beam [8] in a plane (E-plane for this work) to receive a power independent of the radar range for a constant height target. It is also required to have a rapid decrease of the radiation pattern just before the cosecant squared shape in order to not radiate toward the ground. In the orthogonal plane (H-plane), the beam is required to be large to have a nice field of view. Each linear array must operate from 2.62 GHz to 2.69 GHz.

In section 2, we present the design of the patch antenna. In section 3, we detail the design of the feeding network. In section 4, we present simulations of the full linear array, as well as simulations using periodic boundaries to characterize the coupling of the 2D array and simulations of the 4-column array. Finally, in section 5 we present the prototype and its measurements.

II. PATCH ANTENNA DESIGN

The first step in our design is to optimize the patch antenna. This optimization includes the rectangular patch with an inset feed [9], the microstrip line arriving at the patch, a mitered bend and a couple of quarter wavelength transformers. The design with the optimized values is presented in Fig. 1.

Those elements were optimized using CST Studio Suite to maximize the bandwidth of the element around 2.655 GHz, the central frequency of our targeted bandwidth [10].

The substrate used for this design is AD430 from Rogers Corp., with a permittivity equal to 4.3 and a thickness of 3.175 mm. This substrate allows the rectangular patch to have good matching properties over the desired bandwidth [9]. Moreover, using this substrate allows for an element spacing

of approximately 0.56 free space wavelength when using the feeding network architecture presented in the next section.

In Fig. 2, we present the reflection coefficient of the designed patch antenna, which is below -10 dB from 2.61 GHz to 2.69 GHz. The patch antenna presented a gain of 6.5 dB and an efficiency of 80% inside the 2.62 GHz – 2.69 GHz bandwidth.

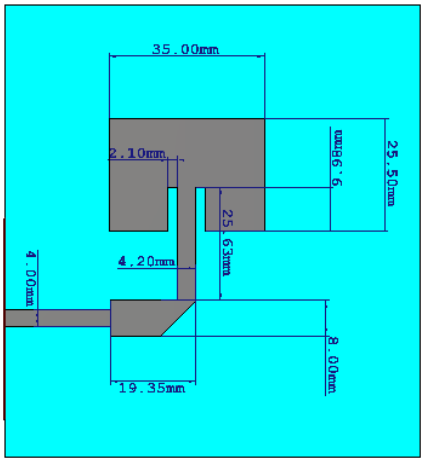

Figure 1. Rectangular patch antenna optimized to maximize its bandwidth around a central frequency of 2.655 GHz.

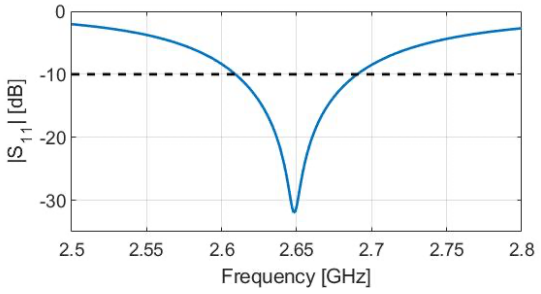

Figure 2. Reflection coefficient of the microstrip antenna presented on Fig. 1.

III. FEEDING NETWORK DESIGN

In this section, we will first present the feeding network architecture used for this antenna array. We will then present the method used to synthesize the parameters of this feeding network, which includes:

- A multi objective genetic algorithm to obtain the currents magnitudes and phases of the array that generate the desired cosecant squared pattern;
- A transmission line model to calculate the lengths and widths of the microstrip lines to obtain those currents magnitudes and phases with the feeding network;
- An iterative procedure using CST Studio Suite to correct the radiating pattern accounting for the different couplings and model imperfections.

A. *PROPOSED ARCHITECTURE*

The proposed feeding network architecture consists of two series of quarter wavelength transformers with T-junctions in between them to feed each of the patch elements and with a bend at the last quarter wavelength transformer to feed the last patch antenna [11].

In between these branches, we have two microstrip lines of unequal electrical lengths, to enforce a phase difference between the two branches, and impedances, to balance the power sent to each of the branches [11].

Both of those microstrip lines arrive at a T-junction that leads to a coaxial feed.

The full architecture with the patch antennas included can be observed in Fig. 3.

B. *MULTI OBJECTIVE GENETIC ALGORITHM*

In order to obtain the desired cosecant squared we used a multi objective genetic algorithm optimization [12]. For this optimization, we considered the set of four consecutive quarter wavelength transformers as equivalent to an amplitude ponderation of the currents on the i^{th} patch in comparison to the $(i-1)^{th}$ patch, with the first patch of each branch normalized to one. As a first approach we consider that the amplitudes on the patches are decreasing the farther we go from the center feed and the maximal reduction is bounded to a third.

TABLE 1: Feeding Network Optimization Parameters

Left Branch			Right Branch			Phase
I_{2left}	I_{3left}	I_{4left}	I_{2right}	I_{3right}	I_{4right}	X_{left} - X_{right}
1.82	1.74	1.09	1.94	1.93	1.09	60°

Moreover, the lines with unequal electrical length on the central feed are equivalent to a phase difference between the currents on left patches and the right patches. Those parameters are summed up in Table I. The indexes of the current magnitudes go from one for the patches closer to the center to four for the outer patches.

For calculating the cost functions below, the radiation pattern of the array was modeled as an Array Factor ($AF(\theta)$) multiplied by a $\cos\theta^q$ model of the element pattern (Eq. 1) for the calculation of the cost functions [13].

$$E_{model}(\theta) = AF(\theta)\ cos^q(\theta) \quad \text{with } q = 3.5 \qquad (1)$$

with the value of q chosen to approximate the element pattern of the patch from Section 2.

The design variables are then optimized to minimize three cost functions:

- one to optimize the formed radiation pattern (Eq. 2):

$$cost_1 = max\left\{20\ log\left[{E_{model}(\theta)}/{csc^2(\theta)}\right]\right\} \qquad (2)$$

for $0° < \theta < 40°$

- one for the sidelobe level (Eq. 3):

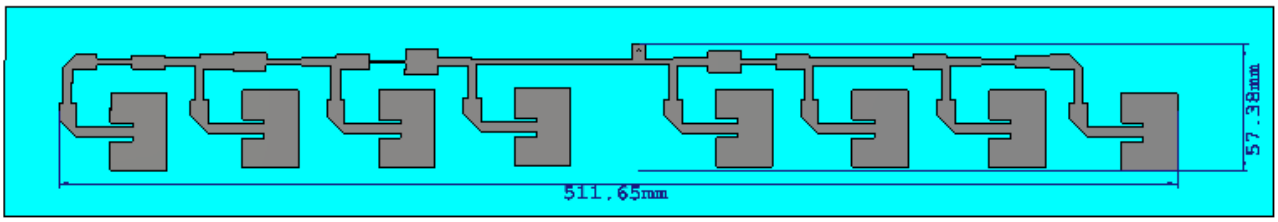

Figure 3: Linear array of microstrip rectangular patches designed following the steps outlined in section III.

$$cost_2 = max\left\{20\,log\left[{E_{model}(\theta)}\Big/{\max E_{model}(\theta)}\right]\right\} \quad (3)$$

for $0° < \theta < 40°$ and $\theta > 40°$

- one for the decrease rate of the main beam of the radiation pattern towards the ground (Eq. 4):

$$cost_3 = \theta_{AFpeak} - \theta_{null} \quad (4)$$

with θ_{AFpeak} corresponding to the maximum of the array factor for θ between 0° and 40° and $\theta_{null} < \theta_{AFpeak}$ the closest angle to θ_{AFpeak} which satisfies Eq. 5:

$$20\,log\left({E_{model}(\theta_{AFpeak})}\Big/{E_{model}(\theta_{null})}\right) = 17\,dB \quad (5)$$

We used the Matlab multi objective genetic algorithms from the Global Optimization Toolbox [14] to optimize this design. The multi objective genetic algorithm gives us 70 dominant solutions for the optimization problem. We restricted these solutions by selection only those which respect the inequalities in Eq. 6.

$$cost_1 < 3dB,\ cost_2 < -10dB,\ cost_3 < 15° \quad (6)$$

We manually selected a solution with a good trade-off between the three cost functions from this reduced set of dominant solutions and the design currents obtained from this solution are presented in Table 1.

C. *FEEDING NETWORK PARAMETER*

Once we calculated the design currents, we moved on to calculating the physical dimensions of the feeding network capable of realizing them. First, we will calculate the impedances of the quarter wavelength transformers needed for this design. Then we will use LineCalc, a Keysight ADS microstrip design tool [15], in order to calculate the physical widths and lengths of each microstrip quarter wavelength transformer.

In order to calculate the impedances we will use Eq. 7, which gives the magnitude of the current on the ith element (I_i) in function of the magnitude of the currents on the (i-1)th element (I_{i-1}) and the impedances of four consecutive quarter wavelength transformers (Z_{c1}, Z_{c2}, Z_{c3} *and* Z_{c4}) [11].

$$\frac{I_{i-1}}{I_i} = \frac{Z_{c1}Z_{c3}}{Z_{c2}Z_{c4}} \quad (7)$$

The indexes of the quarter wavelength transformers in each group of four goes from 1 for the transformers closer to the center of the array to 4 for the ones farther from the center.

We have chosen the impedances of the first and fourth transformer in each group of four quarter wavelength transformers to be equal to, respectively, 70 Ω and 50 Ω. The other two transformers are then calculated to obtain the desired current magnitudes. The impedances of the quarter wavelength transformers are summed up in Table 2.

Concerning the center feed lines we calculated their electrical length in order to realize the phase difference between the patches to the left and to the right of the coaxial feed. As for their impedance, we simulated the full feeding network using ADS and tuned the values in order to balance the power sent to the patches to the left and to the right of the coaxial feed [15].

TABLE 2: Quarter Wavelength Transformer Impedances

Left Branch 1st		Left Branch 2nd		Left Branch 3rd	
Z_{c2_1L}	Z_{c3_1L}	Z_{c2_2L}	Z_{c3_2L}	Z_{c2_3L}	Z_{c3_3L}
50 Ω	65 Ω	52 Ω	65 Ω	65 Ω	51 Ω
Right Branch 1st		Right Branch 2nd		Right Branch 3rd	
Z_{c2_1R}	Z_{c3_1R}	Z_{c2_2R}	Z_{c3_2R}	Z_{c2_3R}	Z_{c3_3R}
50 Ω	69 Ω	50 Ω	69 Ω	65 Ω	51 Ω

D. *ITERATIVE CORRECTION*

Using the patch antenna from Fig. 1 and the feeding network parameters calculated as in the last section we simulated the full array using CST Studio Suite [10].

However, because of coupling effects not taken into account during the design, the amplitude of the currents arriving at the patches does not follow the designed values.

Moreover, the phase difference between the patches to the left and to the right of the coaxial feed is more dependent on frequency then expected from the ADS simulations.

Finally, the resonance frequency of the reflection coefficient is no longer placed at the center of the target bandwidth.

In order to correct the resonance frequency, it is sufficient to slightly change the length of the patches, while proportionally changing the length of the inset feed.

As for the feeding currents, we followed an iterative correction based on the observation of surface currents obtained from the CST simulation:

- We simulate the array using CST with a surface current monitor at the lower, upper and central frequencies (2.62 GHz, 2.655 GHz and 2.69 GHz);
- If the S11 resonance is not centered we fine tune the length of the patches (keeping the inset feed length at the same proportional length);
- We check the radiating pattern at the lower, upper and central frequencies (2.62 GHz, 2.655 GHz and 2.69 GHz). If they are as designed, we stop.
- When look at the surface current RMS value at each of the patches radiating edges at the side further from the feeding network (which is less disturbed by it). We calculate the ratios from one patch to the next and, if the value is different from the prescribed value from Table 1 we change the transformer impedances to compensate this variation. We also check if both central patches have the same RMS current, and if not, we change the impedance of one of the lines in the center of the array to compensate.
- We check the phases of the surface currents at the patches radiating edges to assure the phase difference is as prescribed. If it is not the case, we compensate by varying the length of the transmission lines at the center of the array.

TABLE 3: Feeding Network Physical Dimensions

All values in mm	Z_{c2}		Z_{c3}	
	Length	Width	Length	Width
Transformer 1 Left	14.81	11.90	16.44	0.92
Transformer 2 Left	16.03	2.26	15.12	8.09
Transformer 3 Left	15.34	6.11	15.92	2.71
Transformer 1 Right	14.99	9.47	15.98	2.48
Transformer 2 Right	15.67	3.96	15.82	3.16
Transformer 3 Right	15.88	2.88	15.51	4.94
	Z_{c1}		Z_{c4}	
	Length	Width	Length	Width
All Transformers	15.80	3.36	15.34	6.25
	Left of coaxial feed		Right of coaxial feed	
	Length	Width	Length	Width
Center feed	76.25	1.80	15.88	2.91

In Fig. 4 a flow chart outlining the iterative correction is presented. The parameters of the optimized design are shown in Table 3, and the array front view is presented in Fig. 3.

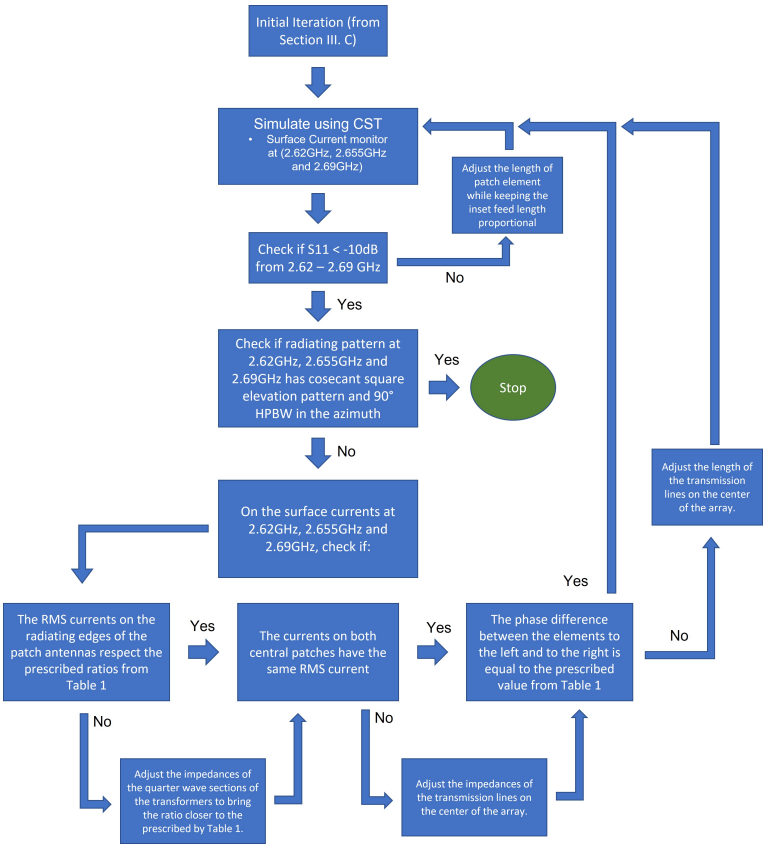

Figure 4: Flow chart outlining the iterative correction of feeding network.

IV. ANTENNA ARRAY SIMULATIONS

In this section we will present the simulation results of the antenna array design following the procedure described in Section 3 (Table 3, Fig. 3). We will first present the results for one isolated column. Then we will include the coupling effects when using several columns side by side in a 2D array by means of periodic boundaries conditions.

A. *SINGLE COLUMN SIMULATION*

In Fig. 5, we show, for the array in Fig. 3, the reflection coefficient and the realized gain in E and H-planes at 2.62 GHz, 2.65 GHz and 2.69 GHz.

As we can see on the E-plane plane, the array presents a slow decrease rate in the realized gain inside of the formed zone, while presenting lobes at least 10 dB than the main beam. The array presents a HPBW of 76° in the H-plane cut. The array has a reflection coefficient bandwidth going from 2.62 GHz to 2.70 GHz. The maximal realized gain of the array goes from 12.3 dB to 13.2 dB in the design bandwidth.

B. *COUPLING EFFECTS*

In Fig. 6, we show, for the array in Fig. 3 calculated with periodic boundaries conditions to obtain an infinite array with a spacing of 65 mm, the reflection coefficient and the realized gain in E and H planes at 2.62 GHz, 2.65 GHz and 2.69 GHz.

As we can see on the E-plane, the array presents a slow decrease rate in the realized gain inside of the formed zone as expected from the results in Fig.5. However, at 2.69 GHz the coupling between the arrays causes a 1.7 dB rise of the sidelobe level.

The array presents a HPBW of 90° in the H-plane cut, 14° larger than the isolated array. The main beam direction is however skewed by 20°.

The array presents a reflection coefficient bandwidth going from 2.62 GHz to 2.71 GHz, slightly larger than that of the isolated array. There is a small drop in the realized gain, which goes from 11.1 dB to 12 dB in the design bandwidth. The coupling between arrays causes this drop.

The performances of the array are not substantially degraded by the presence of neighboring linear arrays, thus this linear array is suitable for use in a 2D array.

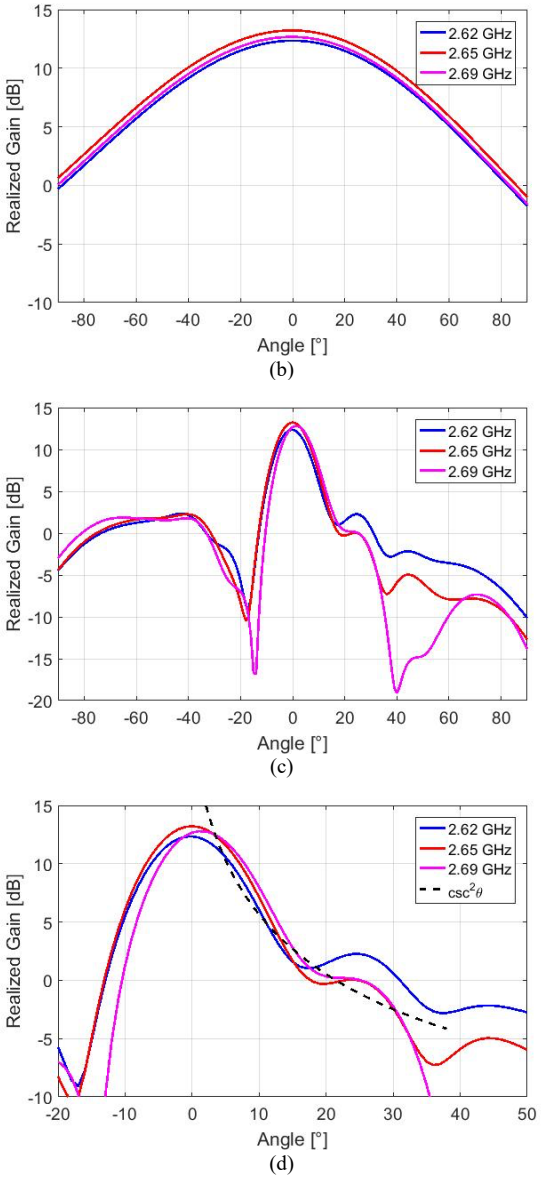

FIGURE 5: Results from the simulation of the array in Fig. 3. In (a) we have the reflection coefficient, in (b) the realized gain in the H-plane, in (c) the realized gain in the E-plane and in (d) a zoom on Fig. 5 (c) with the $csc^2\theta$ pattern superposed for reference.

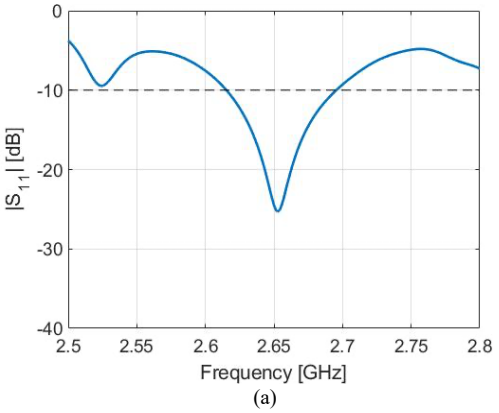

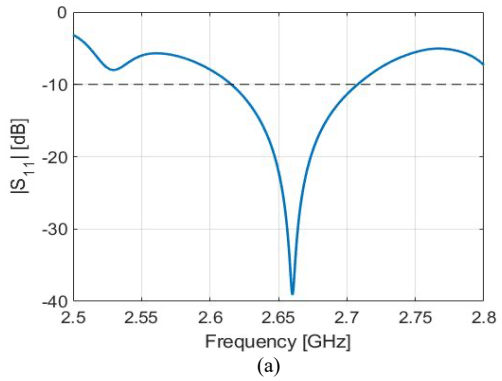

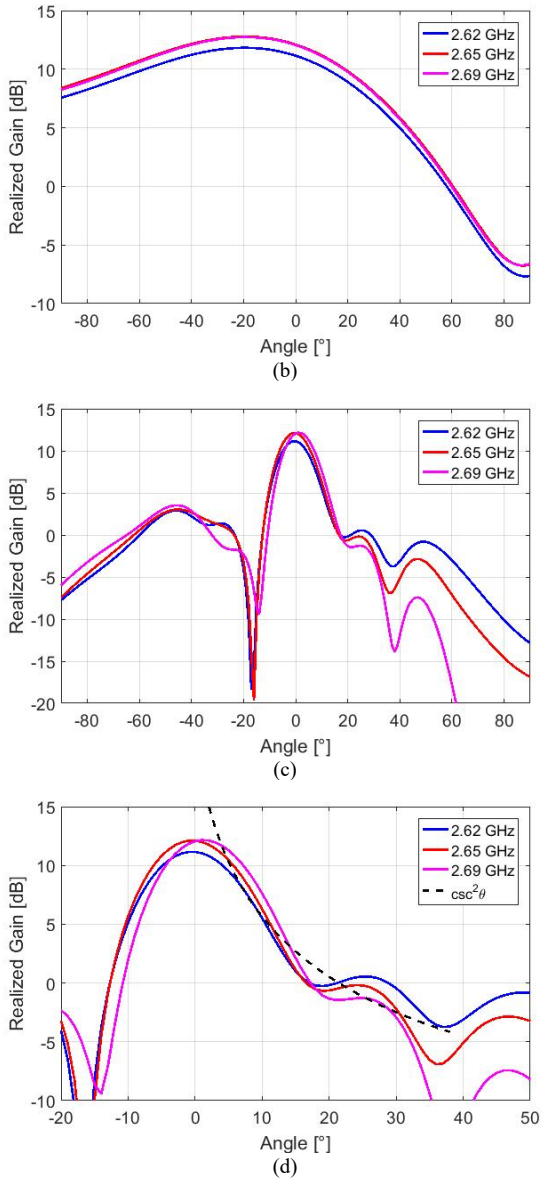

FIGURE 6: Results from the simulation of the array in Fig. 3 with periodic boundaries (spacing between columns equal to 65 mm). In (a) we have the reflection coefficient, in (b) the realized gain in the H-plane, in (c) the realized gain in the E-plane and in (d) a zoom on Fig. 6 (c) with the $csc^2\theta$ pattern superposed for reference.

C. *FOUR COLUMNS SIMULATION*

In Fig. 7, we show the four columns finite array, consisting of four copies of the array in Fig. 3 spaced by 65mm. The column arrays are fed through the center via the connectors labeled J1, J2, J3 and J4.

In Fig. 8, we present the reflection coefficient and the realized gain in E and H planes at 2.62 GHz, 2.65 GHz and 2.69 GHz for this array. As we can see on the E-plane, the array presents a slow decrease rate in the realized gain inside of the formed zone as expected from the results in Fig.5 and Fig. 6. The worst case sidelobe level is below -10 dB.

The array presents a HPBW of 78° in the H-plane cut, closer to that predicted by the isolated array. The main beam direction is however skewed by 8°, less than predicted by the infinite array simulation. The array presents a reflection coefficient bandwidth going from 2.61 GHz to 2.69 GHz. The realized gain goes from 11.6 dB to 12.5 dB in the design bandwidth, in between the values for the single column and the infinite array.

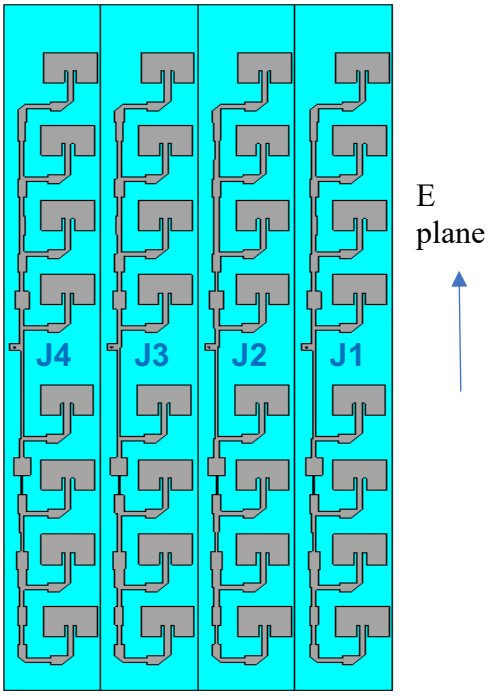

FIGURE 7: 4-column array of microstrip rectangular patches with inset feeds. The array is fed from the center of each column through connectors J1, J2, J3 and J4 via coaxial cables.

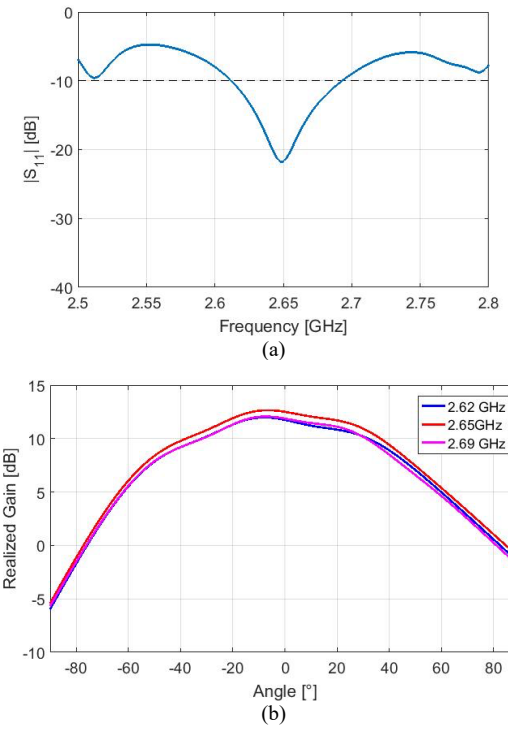

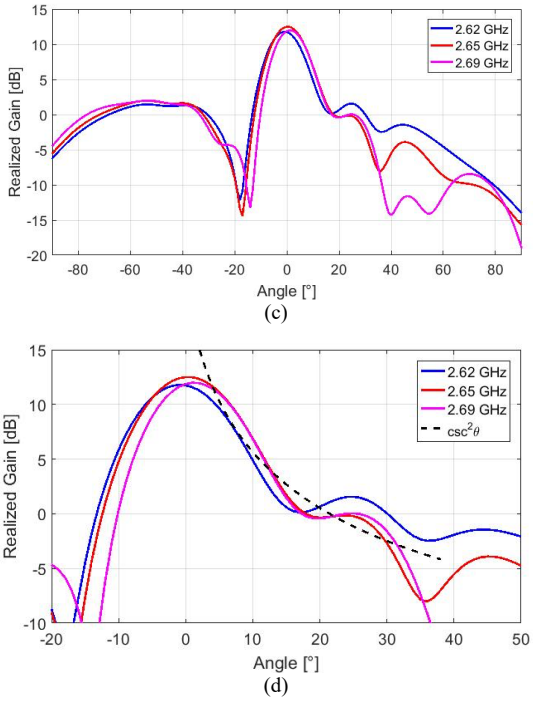

FIGURE 8: Results from the simulation of the array in Fig. 7 (4 times the array in Fig. 3 with spacing between columns equal to 65 mm). In (a) we have the reflection coefficient, in (b) the realized gain in the H-plane, in (c) the realized gain in the E-plane and in (d) a zoom on Fig. 6 (c) with the $csc^2\theta$ pattern superposed for reference.

V. ANTENNA ARRAY PROTOTYPE

The array was designed originally using the AD430 substrate. However, the material became obsolete so we choose to build it using the Kappa438 substrate, which has very similar characteristics to the AD430. The datasheet value for the relative permittivity for this material is 4.38 and the thickness for our prototype is 3.048 mm

As the thickness used for our antenna is not a standard value for this substrate, we built a first prototype of the single column array so that we could obtain the material properties by retrofitting simulations. By closely analyzing the Kappa438 properties, we noticed that it presents a certain level of anisotropy [15]. For our retrofit simulations (Fig. 9), we considered this anisotropy and converged at the value:

$$(\varepsilon_{rx}, \varepsilon_{ry}, \varepsilon_{rz}) = (4.55, 4.55, 4.16), \qquad (8)$$

The first prototype had the bandwidth slightly shifted up from the desired bandwidth and, to correct that, we scaled the entire array by 1.02 (verifying that it did bring the bandwidth to the desired range, 2.62 GHz - 2.69 GHz, by simulating the array using the retrofitted values of the Kappa438).

The antenna compose with four linear arrays was realized and measured in an anechoic chamber. The measurement of the reflection coefficient is given in Fig. 10. Each linear array is measured when 50 Ohms load the others.

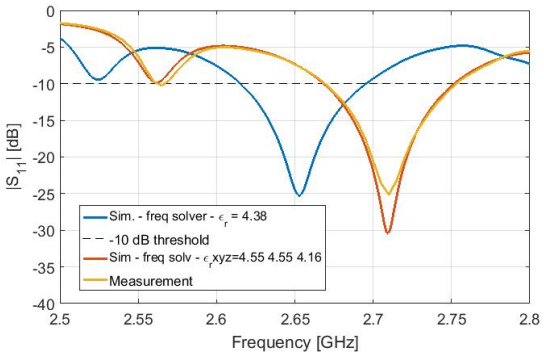

FIGURE 9: Reflection coefficient of the array in Fig. 3 simulated with CST using a $\varepsilon_r = 4.38$ substrate in blue, using a ($\varepsilon_r x$, $\varepsilon_r y$, $\varepsilon_r z$) = (4.55, 4.55, 4.16) substrate in red and the measured prototype first run in yellow.

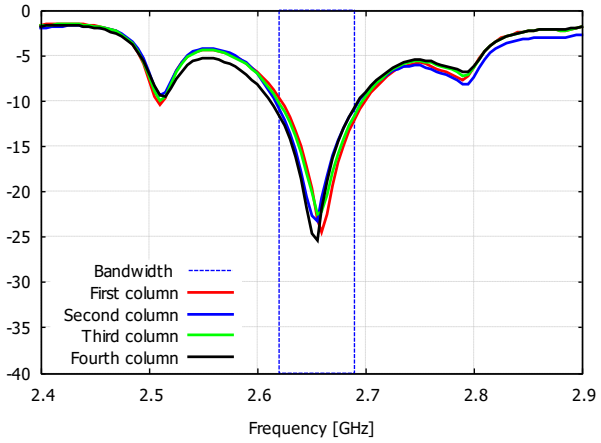

FIGURE 10: Reflection coefficient of one linear array among the three others.

The levels are below -10 dB in the required bandwidth between 2.62 GHz and 2.69 GHz. We can also note a good similarity between the four measurements. The coupling terms were also measured and are less than -20 dB throughout the bandwidth.

The measured radiation patterns in the E plane are plotted in Fig. 11 and compared to the simulations. Only the J3 array is fed (the other arrays being loaded by 50 Ohms).

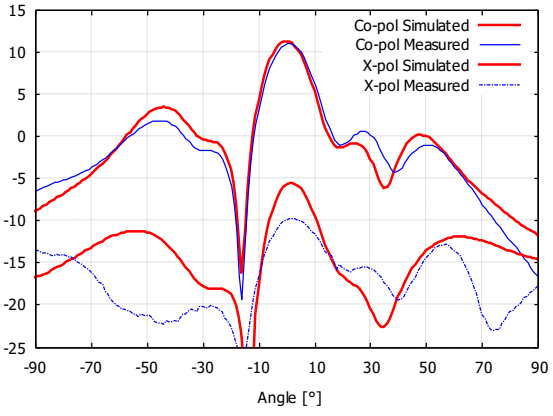

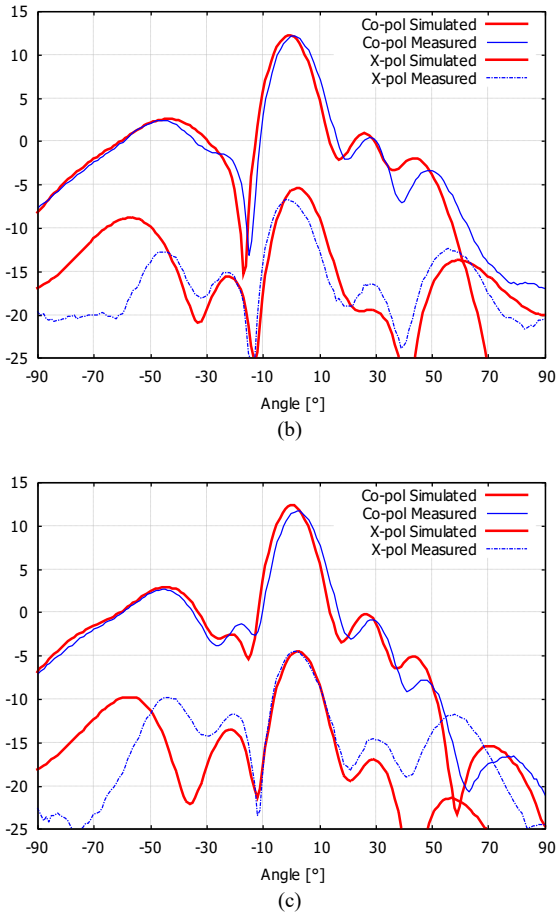

FIGURE 11: Comparison between the measured and simulated E-plane radiation patterns when the connector J3 is fed at 2.62 GHz (a), 2.655GHz (b) and 2.69 GHz (c).

The measured radiation patterns in the H plane are plotted in Fig. 12 and compared to the simulations. Only the J3 array is fed (the other arrays being loaded by 50 Ohms).

For all the measurements, there is good agreement with the simulated results. In E-plane, the shape of the radiation pattern follows the cosecant squared law (towards the sky, positive angles) and the decrease of the radiation pattern is obtained around 15° (towards the ground, negative angles).

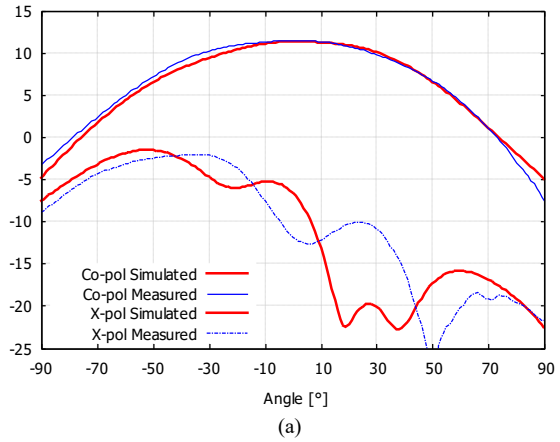

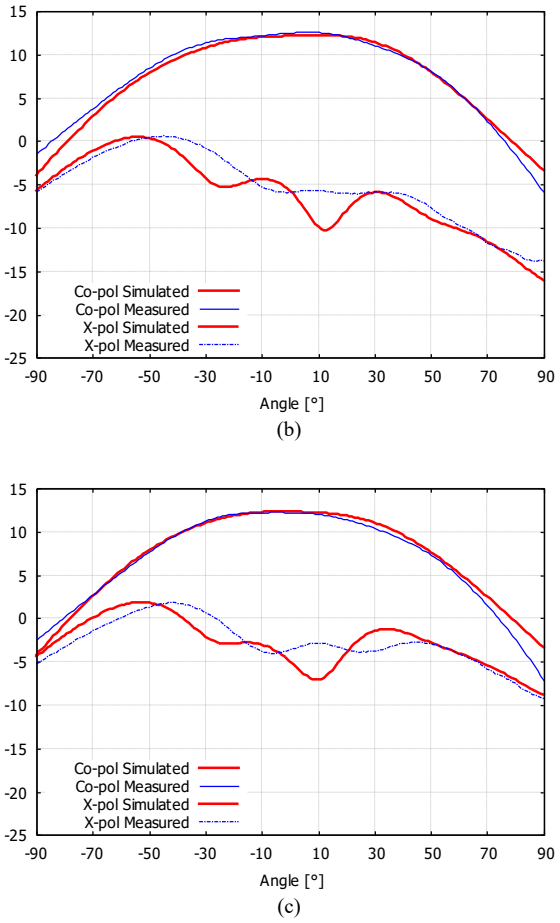

FIGURE 12: Comparison between the measured and simulated H-plane radiation patterns when the connector J3 is fed at 2.62 GHz (a), 2.655GHz (b) and 2.69 GHz (c).

In H-plane, the radiation patterns have HPBW equal to 84° at 2.62 GHz, 88° at 2.655 GHz and 82° at 2.69 GHz. The gain levels vary between 11 dB and 12.9 dB. The cross-polarization components remain 17 dB below the main component on-axis.

VI. CONCLUSION

Four linear arrays of microstrip rectangular patches has been developed and simulated using different simulators. Each linear array has been designed to have a cosecant squared radiation pattern in the E-plane and to presents a 90° HPBW in the H-plane. The design steps procedure has been detailed and a first realization made it possible to take into account the deviations of the materials used. Then four linear arrays have been realized and measured. Each array bandwidth goes from 2.62 GHz to 2.69 GHz with a reflection coefficient below -10 dB and the realized gain that goes from 11.1 dB to 12.2 dB in the required bandwidth. These measurement results, in agreement with the simulation, demonstrate that the arrays have the required specifications in terms of matching and shape of radiation patterns. All of these results validate the design of the four linear arrays.

ACKNOWLEDGMENT

This project has received funding from the Banque Publique d'Investissement and the Conseil Régional d'Ile-de-France (Paris Region) in the framework of the FUI program DIOD.

REFERENCES

[1] S. Park, H. T. Kim, S. Lee, H. Joo and H. Kim, "Survey on Anti-Drone Systems: Components, Designs, and Challenges", *IEEE Access*, vol. 9, pp. 42635-42659, 2021.

[2] M. C. Budge and S. R. German, "Basic Radar Analysis". *Artech House*, 2020.

[3] L. Minz, H. -S. Kang, M. T. Azim, R. S. Aziz and S. -O. Park, "Wide-beam Choke Horn Antenna for Small Drone Detection", *2018 International Symposium on Antennas and Propagation (ISAP)*, Busan, Korea (South), 2018, pp. 1-2.

[4] J. Drozdowicz et al., "35 GHz FMCW drone detection system", *2016 17th International Radar Symposium (IRS)*, Krakow, Poland, pp. 1-4, 2016. doi: 10.1109/IRS.2016.7497351.

[5] M. Caris, W. Johannes, S. Stanko, N. Pohl, "Millimeter Wave Radar for Perimeter Surveillance and Detection of MAVs (Micro Aerial Vehicles)", *Proceedings IRS 2015*, Dresden (Germany), pp284-287, June 2015.

[6] R. K. Miranda, D. A. Ando, J. P. da Costa, and M. T. de Oliveira, "Enhanced direction of arrival estimation via received signal strength of directional antennas", *Proceedings of the 2018 IEEE International Symposium on Signal Processing and Information Technology (ISSPIT)*, pp. 162–167, 2018.

[7] D. A. Ando, R. K. Miranda, J. P. da Costa, and M. T. de Oliveira, "A novel direction of arrival estimation algorithm via received signal strength of directional antennas", *Proceedings of the 2018 Workshop on Communication Networks and Power Systems (WCNPS)*, pp. 1–5, 2018.

[8] R. C. Hansen, "Array pattern control and synthesis", *Proc. IEEE*, vol. 80, pp. 141-151, Jan. 1992.

[9] J. L. Volakis, "Antenna Engineering Handbook", *4th Edition, McGraw-Hill Education*, 2014.

[10] CST Studio Suite 2016.

[11] D. M. Pozar, "Microwave Engineering", *4th Edition, John Wiley & Sons*, 2012.

[12] R. L. Haupt, D. H. Werner, "Genetic Algorithms in Electromagnetics", *John Wiley & Sons*, 2006.

[13] R. L. Haupt, "Antenna Arrays, a Computational Approach", *John Wiley & Sons*, 2010.

[14] Matlab 2018 Global Optimization Toolbox.

[15] ADS 2018 Keysight.

[16] MWI Microwave Impedance Calculator, Rogers Corporation, 2019.